Effect of MHD on Porous Circular Stepped Plate Lubricated With Micropolar Fluid

Johny. A, Sujatha. E and Geetha Sree. M

***Abstract*—An analysis is made on the effect of magneto hydrodynamics on poro-circular stepped plates lubricated with micropolar fluid. The modified Reynold's equation leads to the development of a closed form expression for pressure, load sustaining capacity, and squeezing time. The impact of porosity is analyzed using the modified Darcy's equation, and the outcomes are compared with the cases of the presence and absence of porosity on the same circular stepped plate. The external magnetic field influences the bearing's efficiency by increasing the pressure, load sustaining capacity, and squeezing time performance. In the presence of porosity, the pressure, load sustaining capacity and squeezing time decrease compared to the absence of porosity, and the comparisons are shown in the tables. The variation of the highly influenced parameter of the bearing system is represented graphically.**

***Index Terms*—Micropolar fluid, porosity, circular stepped plate, MHD, Relative percentage.**

I. Introduction

MAGNETOHYDRODYNAMICS deals with the study of magnetic properties and electrically conducting fluid behavior. Hannes Alfven developed the MHD field. The underlying opinion at the heels of MHD is that magnetic fields may generate currents in a fluid that is flowing conductively, polarizing the fluid and wavering itself. MHD is characterized by Navier-Stoke's equation and Maxwell's equation of electromagnetism, which are found either numerically or analytically. In biological systems, as a field of science, MHD involves the physiological fluids that are electrically conducting under the action of exerted magnetic fields. Biomagnetic fluids are considered working fluids in medical science. MHD mathematical equations and finite element analysis are passed down to examine the magnetic fluid particle's interaction in the blood flow. Based on this principle, many researchers were inspired to work on MHD. Jung and Lee [1] studied about the pumping mechanism for a novel micro pump based on the MHD principles both theoretically and experimentally. Bujurke and Kudenatti [2] analyzed the flow of MHD lubrication within rough rectangular plates and it was noticed that the influence of roughness and magnetic field was to optimize the load sustaining capacity and therefore delaying squeezing time. Lin [3] and Hayat et al [4] studied MHD squeezing film characteristics between annular disks and the squeezing flow of micropolar fluid, which is lubricated within parallel disks, respectively. The utility of lubricants like non-Newtonian fluids has recently captured demand. Randomly oriented particles floating in a viscous liquid with no consideration for particle deformation and fluids with microstructures are called micropolar fluids. Further covering both theory and applications, there is a micro-rotational phenomenon in a micropolar fluid. The internal particles of fluid may alter in area and shape; their geometry may reduce or expand. Over and above that, they can rotate on their own. They can also move unrestricted through bulk flow. Animal blood and liquid crystals represent complex fluids with microstructures, which come under the category of micropolar fluids. Not only couple stresses, but they can also benefit the surface and the body as these fluids respond to micro-rotational motions. The theory of micropolar fluid investigates the origin of micropolar fluid, which was introduced by Eringen [5]. Laminar fluid behavior was studied using the micropolar fluid theory that was proposed by Papautsky et.al [6]. In this paper, they predicted the behavior of fluid in microchannels using the micropolar fluid theory, which they also verified experimentally on micromachined channels.

Bearings are the process of mechanical assemblies that consist of elements that are in rotating motion, and in certain cases both internal and external races are used for applications of rotating shafts. Aside from ball bearings, there are several other types of bearings. Ball bearings contain rolling factors, which are used for lighter weight applications, whereas rolling element bearings have cylindrical rolling elements which are used for bulkier weight-bearing demands. Linear bearings are used for linear motions along shafts and may also have rotating potential. Interestingly, the automotive sector has accounted for the demand for bearing manufacturers in recent times. Research and development (RD)-bearing companies are even increasing investments. The various bearing configurations are thrust, step, slider, hydrodynamic bearings, and hydrostatic bearings. Needle roller bearing is the most sought after bearing in which RD wing of much companies are working on. Micropolar lubricant influence the performance of bearings was studied by Khatak and Garg [7]. In general, porosity plays a crucial role in squeeze film characteristics. Based on permeability, porosity influences the flow by accelerating or decelerating. Many of the researchers showed interest in porous as they are relatively inexpensive and geomentry which is easy to handle. Porous bearings are commonly employed in general equipment because of their self-lubricating properties and load carrying capacity. Based on the application requirement lubricant can be either solid or liquid. Compared to other dry sliding bearings self lubricating porous bearings are more advantageous due to constant oil presence avoids the seizure risk and improves wear efficiency.

Manuscript received Januray 29, 2024; revised June 25, 2024.

Johny.A is a Research Scholar in the Department of Mathematics, College of Engineering and Technology, SRM Institute of Science and Technology, Kattankulathur 603203, Tamil Nadu, India (e-mail:ja4545@srmist.edu.in).

Sujatha. E is an Assistant Professor in the Department of Mathematics, College of Engineering and Technology, SRM Institute of Science and Technology, Kattankulathur 603203, Tamil Nadu, India (Corresponding author; phone:9884708590; e-mail:sujathae@srmist.edu.in).

Geetha Sree. M is a Post Graduate student in the Department of Mathematics, College of Engineering and Technology, SRM Institute of Science and Technology, Kattankulathur 603203, Tamil Nadu, India (e-mail:mg5961@srmist.edu.in).

Johny and Sujatha [8] investigated the work of a rough-porous Rayleigh step slider bearing with the MHD effect lubricated by couple stress fluid and it was compared to a porous rough step slider with the MHD effect. Biplab Bhattacharjee et.al [9] found that, when compared to other traditional lubricants, a single layer porous journal bearing where micropolar fluid is lubricated had a high load sustaining capacity. Johny and sujatha [23] worked on the double porous based step slider bearing. In order to support the load, the squeeze film phenomenon originates in a normal direction when two lubricating layers move towards each other, which generates positive pressure. Based on this phenomenon, several authors like Naduvinamani and Santosh [10], Naduvinamani and Siddangouda [11], and Shah [12] have investigated the performance of squeeze film lubrication in bearings such as journal bearings and circular stepped plates. In addition, Naduvinamani and Shridevi [13] examined this squeeze film lubrication with the effect of MHD between porous parallel plates.

Further, based on pressure dependent viscosity load carrying capacity is examined by Birenda and Pentyala [14] and Hanumagowda et.al [15]. Through these [14], [15] it has been found that an increase in non dimensional stepped distance decreases the dimensionless load sustaining capacity, pressure and time. Nayak [19] worked on the unsteady third grade fluid with viscous dissipation, where it was found that the magnetic parameter M values rise, temperature rises, and velocity falls. Salah and Elhabian [17] analyzed the effect of second-grade fluid flow over stretching sheet, where as the Hartman number M and Prandtl number Pr rise, and the velocity and temperature fields decrease. The MHD effect within circular stepped plates lubricated with a couple stress fluids was analyzed by Naduvinamani et.al [16]. According to the findings, applying an external magnetic field improves load sustaining capacity and obstructs the time approach in comparison with the case of a non-magnetic field. Brinda et.al [18] examined the significance of surface roughness with the MHD effect within two porous elliptical plates. Recently, Sangeetha et.al [21] studied conical rough bearings with the effect of MHD lubricated by micropolar fluid and observed that as coupling number and Hartman number values increase, there is an enhancement in squeeze film characteristics. Faizan Ahmed and Sujatha [24] analyzed the effect of surface roughness on the porous triangular plate. It is found that the induced magnetic field increases the workload compared to a similar condition without a magnetic field. Furthermore, Naduvinamani and Angadi [22] also studied the influence of micropolar fluid and MHD between stepped porous parallel plates. In this paper [22], it is found that the magnetic field influence helps to enhance the workload. Johny and sujatha [20] worked on the circular stepped plated which is lubricated with micropolar fluid and the surface of the plate is considered smooth.

According to a review of the literature, no work has been made to explore the influence of magnetohydrodynamics (MHD) on porous circular stepped plates where micropolar fluid is used as lubricant. The aim was to analyze the system with and without porosity and find that the bearing is more efficient in the absence of porosity. Here, the load sustaining capacity and the squeezing time are derived and analyzed by varying the parameters like M (Hartman number), N (coupling number), L (characteristic material length), ψ permeability, and K step height of the bearing. Through the influence of Hartman number and coupling number the load sustaining capacity and the squeezing time are enhanced.

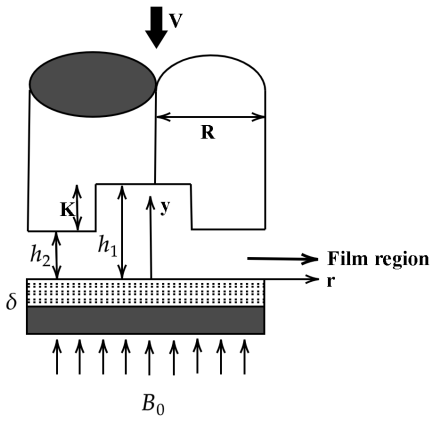

Fig. 1. Geometry of porous circular stepped plate

II. Geometry of the Bearing

The physical illustration of a circular stepped plate is given in Fig.1. The upper plate moves toward the lower plate with squeezing velocity $V = \frac{dh}{dt}$. Consider R as the radius of the circular plate which has a step in the center which is of height K. The micropolar fluid is considered a lubricant used between circular stepped plates, which flows in the direction of r, where the maximum film thickness is h_1 and the minimum film thickness is h_2. Here the lower plate is porous in nature with layer thickness δ. The circular plates is subjected to the constant magnetic field B_0 which acts in a perpendicular direction (direction of y) to the fluid flow.

Assuming the basic assumptions of thin film lubrication to hold true, the governing equations of a micropolar fluid are given as follows:

Linear momentum:

$$\left(\frac{2\mu+\chi}{2}\right)\frac{\partial^2 u}{\partial y^2}+\chi\frac{\partial v_1}{\partial y}-\sigma B_0^2 u=\frac{\partial p}{\partial r} \tag{1}$$

Angular momentum:

$$\gamma\frac{\partial^2 v_1}{\partial y^2}-2\chi v_1-\chi\frac{\partial u}{\partial y}=0 \tag{2}$$

Mass:

$$\frac{1}{r}\frac{\partial(ru)}{\partial r}+\frac{\partial v}{\partial y}=0 \tag{3}$$

and

$$\frac{\partial p}{\partial y}=0 \tag{4}$$

In the above equations, u and v represent the velocity components in the direction of r and y respectively; v_1 is micro-rotational velocity, B_0 denotes the strength of the magnetic field; σ represents the electrical conductivity of the fluid, μ represents the viscosity of the micro-polar fluid, χ represents its spin viscosity and γ represents its viscosity coefficient. The film thickness H between the plates is considered in the following form:

$$H=\begin{cases} h_1 & \text{for} \quad 0\le r\le KR \\ h_2 & \text{for} \quad KR\le r\le R \end{cases}$$

For the velocity components, the necessary boundary conditions are:
(i) On the lower porous surface $y = 0$

$$u = 0, v = -v^*, v_1 = 0 \tag{5}$$

(ii) On the upper surface $y = H$

$$u = 0, v = V, v_1 = 0 \tag{6}$$

By solving the equation (1) and (2) and using boundary conditions (5) and (6) the velocity component u is derived as.

$$u = \frac{a-b}{\sigma B_0^2[c-d]}\frac{\partial p}{\partial r} \tag{7}$$

where
$a = g_1 \sinh(k_1 H)[\cosh(k_2 H) - \cosh(k_2 y)]$
$b = g_2 \sinh(k_2 H)[\cosh(k_1 H) - \cosh(k_1 y)]$
$c = g_2 \sinh(k_2 H)\cosh(k_1 H)$
$d = g_1 \sinh(k_1 H)\cosh(k_2 H)$
Darcy's permeability is characteristic of the porous medium and the fluid flowing through it. Laplace's rule says that the pressure inside an inflated elastic container with a curved surface is equal to the pressure outside. Based on these laws, the expression for pressure is derived.
The modified Darcy's equation is given as

$$\overrightarrow{q} = (u^*, v^*) = \frac{-\phi^*}{\mu + \chi}\ \nabla p^* \tag{8}$$

Here, u^* and v^* are the velocity components in the porous region in r and y direction respectively. pressure in the permeable region is denoted as p^* and ϕ^* is porous permeability. From the Laplace equation which is satisfied by p^*,

$$\frac{\partial^2 p^*}{\partial r^2} + \frac{\partial^2 p^*}{\partial y^2} = 0 \tag{9}$$

By integrating equation(9) with respect to y and applying the boundary condition at $y = -\delta$, $\frac{\partial p^*}{\partial y} = 0$ then we get,

$$\left(\frac{\partial p^*}{\partial y}\right)_{y=0} = \int_{-\delta}^{0} \frac{\partial^2 p^*}{\partial r^2} dy \tag{10}$$

At $y = 0$ the velocity component v^* is given by

$$[v^*]_{y=0} = \frac{\phi^* \delta}{\mu + \chi}\left(\frac{\partial^2 p}{\partial r^2}\right) \tag{11}$$

By using the expression of u and integrating the equation (3) w.r.to y over a film thickness the modified Reynold's equation is obtained as

$$\frac{\partial}{\partial r}\left[\left(f(H,N,L,M) + \frac{\phi^* \delta}{\mu + \chi}\right) r \frac{\partial p}{\partial r}\right] = -Vr \tag{12}$$

In non-dimensional form, the modified Reynold's equation is of the form

$$\frac{\partial}{\partial \overline{r}}\left[\left(F(H,N,L,M) + \psi\left(\frac{1-N^2}{1+N^2}\right)\right)\overline{r}\frac{\partial \overline{p}}{\partial \overline{r}}\right] = -\overline{r} \tag{13}$$

where $F(H,N,L,M) = \frac{a_1 - b_1}{M^2 \overline{k_1} \overline{k_2}(c_1 - d_1)}$,
$a_1 = \overline{g_1}\,\overline{k_1} \sinh(\frac{\overline{k_1} H}{2})(\overline{k_2} H \cosh(\frac{\overline{k_2} H}{2}) - 2\sinh(\frac{\overline{k_2} H}{2}))$,
$b_1 = \overline{g_2}\,\overline{k_2} \sinh(\frac{\overline{k_2} H}{2})(\overline{k_1} H \cosh(\frac{\overline{k_1} H}{2}) - 2\sinh(\frac{\overline{k_1} H}{2}))$,
$c_1 = \overline{g_1} \cosh(\frac{\overline{k_2} H}{2})(\sinh(\frac{\overline{k_1} H}{2}))$,
$d_1 = \overline{g_2} \cosh(\frac{\overline{k_1} H}{2})(\sinh(\frac{\overline{k_2} H}{2}))$,
$\overline{g_1} = \frac{M^2(1-N^2) - \overline{k_1}^2}{2N^2 \overline{k_1}}$, $\overline{g_2} = \frac{M^2(1-N^2) - \overline{k_2}^2}{2N^2 \overline{k_2}}$,
$\overline{k_1} = \sqrt{\frac{\overline{\alpha} + \sqrt{\overline{\alpha}^2 - 4\overline{\beta}}}{2}}$, $\overline{k_2} = \sqrt{\frac{\overline{\alpha} - \sqrt{\overline{\alpha}^2 - 4\overline{\beta}}}{2}}$,
$\overline{\alpha} = \frac{N^2 + M^2(1-N^2)L^2}{L^2}$, $\overline{\beta} = \frac{N^2 M^2}{L^2}$,
$M = B_0 h_2 \sqrt{\frac{\sigma}{\mu}}$, $L = \frac{\sqrt{\frac{\gamma}{4\mu}}}{h_2}$, $N = \sqrt{\frac{\chi}{2\mu + \chi}}$.
Here the non-dimensional quantities are as follows
$\overline{r} = \frac{r}{R}$, $\overline{\alpha} = h_2^2 \alpha$, $\overline{\beta} = h_2^4 \beta$, $\overline{g_1} = h_2 g_1$, $\overline{g_2} = h_2 g_2$
$\psi = \frac{\phi^* \delta}{h_2^3}$, $T = \frac{W t h_2^2}{\mu_0 R^4}$, $\overline{p} = \frac{p h_2^3}{\mu R^2 V}$
where M is Hartman parameter, N is dimensionless coupling number, L is characteristic material length.
The related boundary conditions of pressure are given below,

$$\overline{p_1} = \overline{p_2}\ at\ \overline{r} = K \tag{14}$$

$$\overline{p_2} = 0\ at\ \overline{r} = 1 \tag{15}$$

By solving equation (13) using the conditions equation (14) and equation (15) we get

$$\frac{\partial \overline{p}}{\partial \overline{r}} = \frac{-\overline{r}}{2\left(F(H,N,L,M) + \psi\left(\frac{1-N^2}{1+N^2}\right)\right)} \tag{16}$$

On integrating the Equation (16) the dimensionless expression of pressure is obtained as

$$\overline{p_1} = \frac{K^2 - \overline{r}^2}{4F_1(\overline{h_1}, N, L, M, \psi)} + \frac{1 - K^2}{4F_2(1, N, L, M\psi)} \tag{17}$$

$$\overline{p_2} = \frac{1 - \overline{r}^2}{4F_2(1, N, L, M, \psi)} \tag{18}$$

The load sustaining capacity w is given as

$$w = 2\pi \int_0^{KR} r(p_1) dr + 2\pi \int_{KR}^{R} r(p_2) dr \tag{19}$$

By solving Equation (19) the load sustaining capacity W in dimensionless form is got as

$$W = \frac{K^4}{8F_1(\overline{h_1}, N, L, M, \psi)} + \frac{1 - K^4}{8F_2(1, N, L, M, \psi)} \tag{20}$$

The squeezing time required to reduce the initial thickness h_0 of h_2 to final film thickness h_f of h_2 by substituting $V = \frac{dh}{dt}$ is

$$T = \int_{h_f}^{1} \left(\frac{K^4}{8G_1(N, \overline{h}_s, \overline{h}_2, L, M, \psi)} + \frac{1 - K^4}{8G_2(N, \overline{h}_2, L, M, \psi)}\right) dh_2 \tag{21}$$

where $G_1(N, \overline{h}_s, \overline{h}_2, L, M) = \frac{a_2 - b_2}{M^2 \overline{k_1} \overline{k_2}(c_2 - d_2)}$
$a_2 = \overline{g_1}\,\overline{k_1} \sinh\left(\frac{\overline{k_1}(\overline{h}_s + \overline{h}_2)}{2}\right)\left(\overline{k_2}(\overline{h}_s + \overline{h}_2)\cosh(\frac{\overline{k_2}(\overline{h}_s + \overline{h}_2)}{2}) - 2\sinh\left(\frac{\overline{k_2}(\overline{h}_s + \overline{h}_2)}{2}\right)\right)$
$b_2 = \overline{g_2}\,\overline{k_2} \sinh\left(\frac{\overline{k_2}(\overline{h}_s + \overline{h}_2)}{2}\right)\left(\overline{k_1}(\overline{h}_s + \overline{h}_2)\cosh(\frac{\overline{k_1}(\overline{h}_s + \overline{h}_2)}{2}) - 2\sinh\left(\frac{\overline{k_1}(\overline{h}_s + \overline{h}_2)}{2}\right)\right)$
$c_2 = \overline{g_1}\cosh\left(\frac{\overline{k_2}(\overline{h}_s + \overline{h}_2)}{2}\right)\sinh\left(\frac{\overline{k_1}(\overline{h}_s + \overline{h}_2)}{2}\right)$
$d_2 = \overline{g_2}\cosh\left(\frac{\overline{k_1}(\overline{h}_s + \overline{h}_2)}{2}\right)\sinh\left(\frac{\overline{k_2}(\overline{h}_s + \overline{h}_2)}{2}\right)$
$G_2(N, \overline{h}_2, L, M) = \frac{a_3 - b_3}{M^2 \overline{k_1} \overline{k_2}(c_3 - d_3)}$

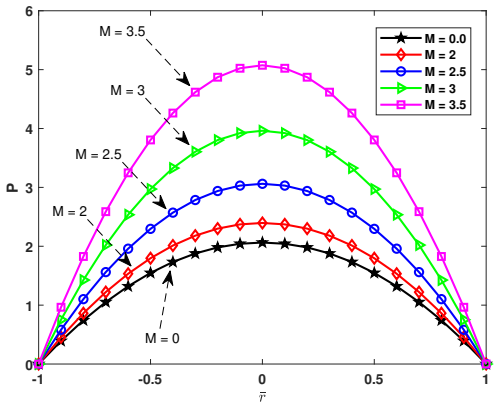

Fig. 2. Plot of dimensionless pressure P versus $\overline{r}$ for different values of M

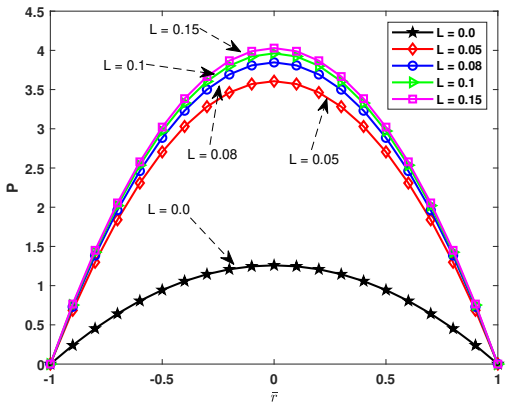

Fig. 4. Plot of dimensionless pressure P versus $\overline{r}$ for different values of L

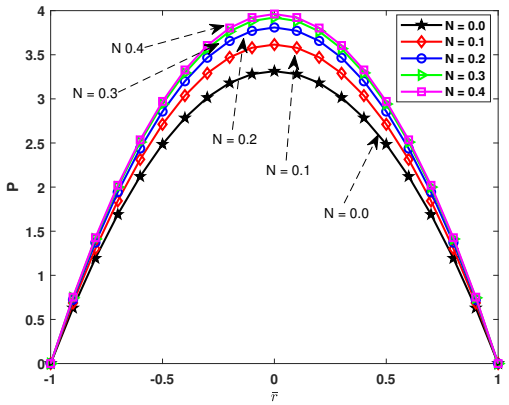

Fig. 3. Plot of dimensionless pressure P versus $\overline{r}$ for different values of N

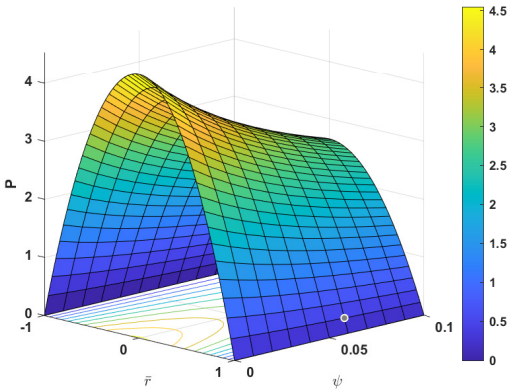

Fig. 5. Surface plot of dimensionless pressure P by varying $\overline{r}$ and ψ

$$a_3 = \overline{g_1}\overline{k_1}\sinh\left(\frac{\overline{k_1}\overline{h_2}}{2}\right)\left(\overline{k_2}\overline{h_2}\cosh\left(\frac{\overline{k_2}\overline{h_2}}{2}\right) - 2\sinh\left(\frac{\overline{k_2}\overline{h_2}}{2}\right)\right)$$

$$b_3 = \overline{g_1}\overline{k_2}\sinh\left(\frac{\overline{k_2}\overline{h_2}}{2}\right)\left(\overline{k_1}\overline{h_2}\cosh\left(\frac{\overline{k_1}\overline{h_2}}{2}\right) - 2\sinh\left(\frac{\overline{k_1}\overline{h_2}}{2}\right)\right)$$

$$c_3 = \overline{g_1}\cosh\left(\frac{\overline{k_2}\overline{h_2}}{2}\right)\sinh\left(\frac{\overline{k_1}\overline{h_2}}{2}\right)$$

$$d_3 = \overline{g_2}\cosh\left(\frac{\overline{k_1}\overline{h_2}}{2}\right)\sinh\left(\frac{\overline{k_2}\overline{h_2}}{2}\right)$$

$$F_1(\overline{h_1}, N, L, M) + \psi\left(\frac{1-N^2}{1+N^2}\right) = F_1(\overline{h_1}, N, L, M, \psi)$$

$$F_2(1, N, L, M) + \psi\left(\frac{1-N^2}{1+N^2}\right) = F_2(1, N, L, M, \psi)$$

$$G_1(N, \overline{h}_s, \overline{h}_2, L, M) + \psi\left(\frac{1-N^2}{1+N^2}\right) = G_1(N, \overline{h}_s, \overline{h}_2, L, M, \psi)$$

$$G_2(N, \overline{h}_2, L, M) + \psi\left(\frac{1-N^2}{1+N^2}\right) = G_2(N, \overline{h}_2, L, M, \psi)$$

III. Results and Discussions

The parameters characteristic length L, coupling number N, Hartman number M, and permeability parameter ψ define the impact of MHD and micropolar fluid on the squeeze film performance of porous circular stepped plates. It is noted that the problem is examined in the cases of $\psi = 0$ (in the absence of porous) and $\psi = 0.01$ (in the presence of porous). A table displays the differences between the presence and absence of porous materials. It analyzes the graphical representation to understand the impact of pressure P, load carrying capacity W, and squeeze film time T. To understand the permeability ψ performance in the circular stepped plate, Fig. 5, 10, 11, 12 17 and 18 display the variations as three-dimensional surface plots.

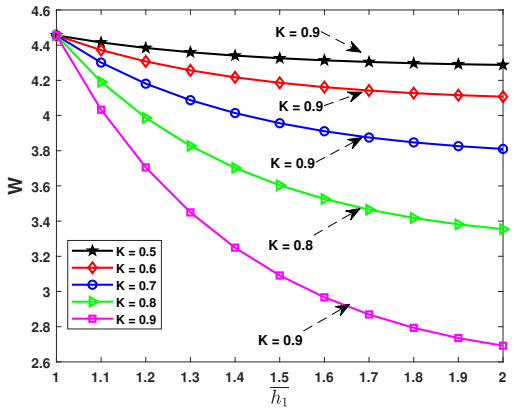

Fig. 6. Plot of dimensionless work load W versus $\overline{h_1}$ for different values of K

A. Dimensionless Pressure

The dimensionless pressure varied with axial distances $\overline{r}$ for different values of specified parameters, like M, N, L, and ψ, as shown in fig 2, 3, 4, and 5, respectively. Fig 2, 3, and 4 show that the effect of pressure P increases while increasing the parameters M, N, and L, respectively. In fig 4 and 5, pressure decreases while increasing the parameters K and ψ.

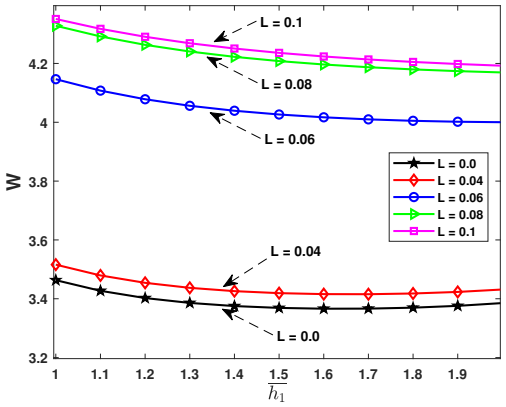

Fig. 7. Plot of dimensionless work load W versus $\overline{h_1}$ for different values of L

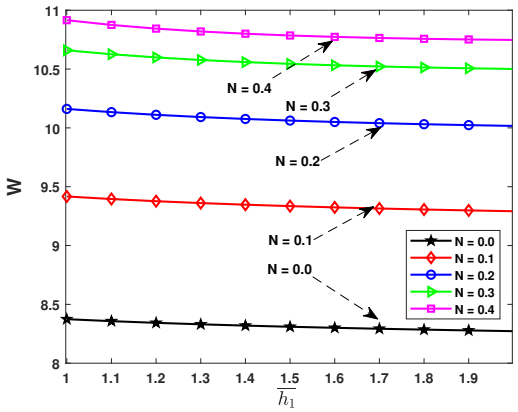

Fig. 8. Plot of dimensionless work load W versus $\overline{h_1}$ for different values of N

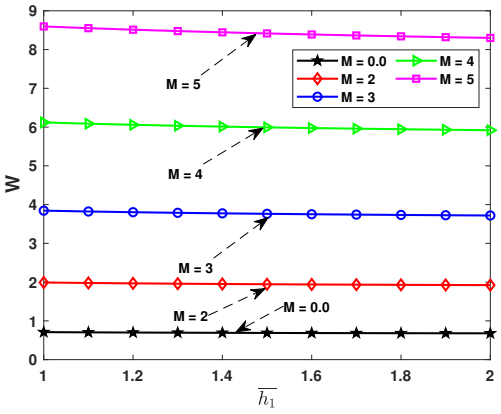

Fig. 9. Plot of dimensionless workload W versus $\overline{h_1}$ for different values of M

B. Dimensionless Load sustaining capacity

The dimensionless load sustaining capacity is varied with dimensionless film thickness $\overline{h_1}$ for different values of specified parameters like L, N, M, K, and ψ. It is compared between the porous and non-porous cases, observing that the non-porous case has a greater load than the porous case. As shown in fig 6, the plot of dimensionless load W versus maximum film thickness $\overline{h_1}$ varied with different values of step distance K. It has been discovered that the load-

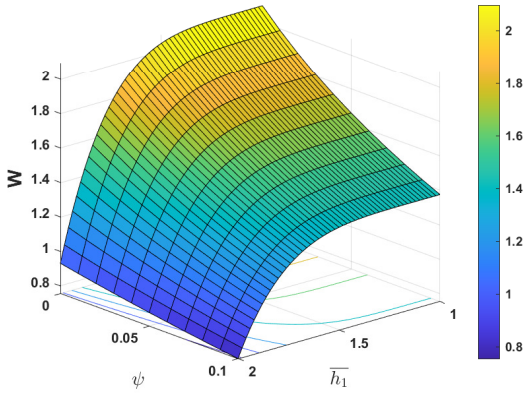

Fig. 10. Surface plot of dimensionless workload W by varying $\overline{h_1}$ and ψ

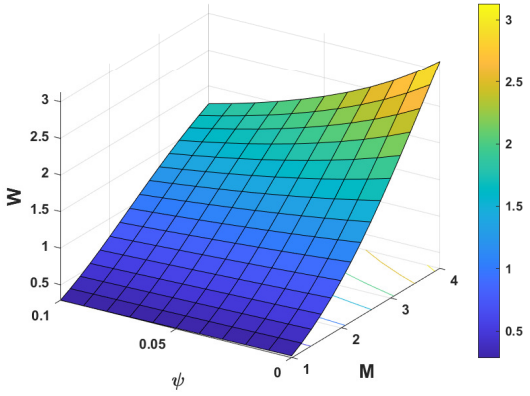

Fig. 11. Surface plot of dimensionless workload W by varying M and ψ

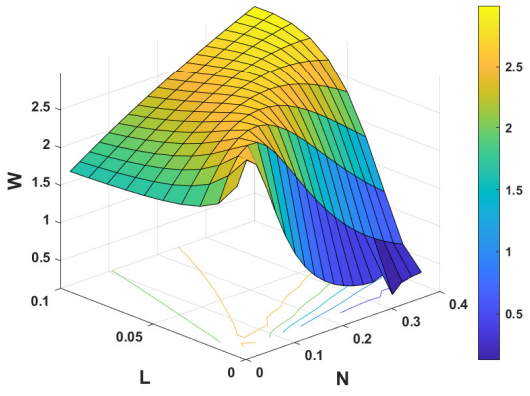

Fig. 12. Surface plot of dimensionless workload W by varying L and N

TABLE I
COMPARISON BETWEEN POROUS AND NON POROUS CASES ON LOAD SUSTAINING CAPACITY FOR VARIOUS VALUES OF K AND L

	$\overline{h_1}$	1.2	1.4	1.6	1.8	2
ψ=0.01	L = 0.05	3.4541	3.4259	3.4158	3.4179	3.4315
	L = 0.06	4.0783	4.0392	4.0169	4.0050	4.0002
	L = 0.08	4.2633	4.2225	4.1965	4.1798	4.1694
ψ=0.0	L = 0.05	3.7294	3.6982	3.6871	3.6895	3.7043
	L = 0.06	4.4673	4.4233	4.3987	4.3857	4.3805
	L = 0.08	4.6899	4.6435	4.6145	4.5963	4.5850
ψ=0.01	K = 0.6	4.3074	4.2172	4.1615	4.1273	4.1072
	K = 0.7	4.1810	4.0140	3.9108	3.8474	3.8102
	K = 0.8	3.9872	3.7023	3.5263	3.4181	3.3547
ψ=0.0	K = 0.6	4.6824	4.5816	4.5206	4.4836	4.4621
	K = 0.7	4.5358	4.3490	4.2360	4.1674	4.1276
	K = 0.8	4.3110	3.9921	3.7994	3.6825	3.6146

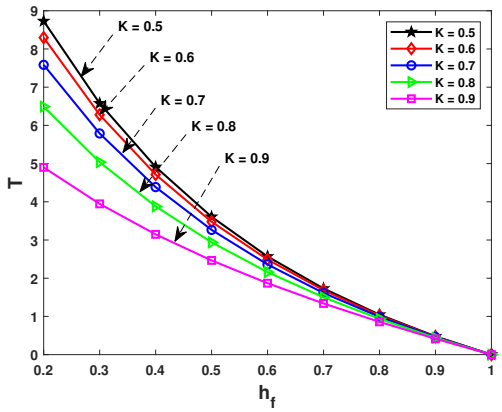

Fig. 13. Plot of dimensionless time T versus h_f for different values of K

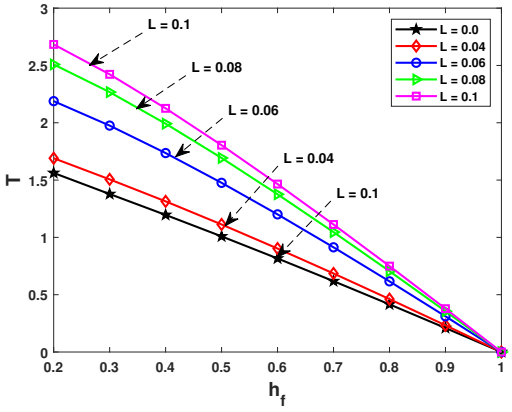

Fig. 14. Plot of dimensionless time T versus h_f for different values of L

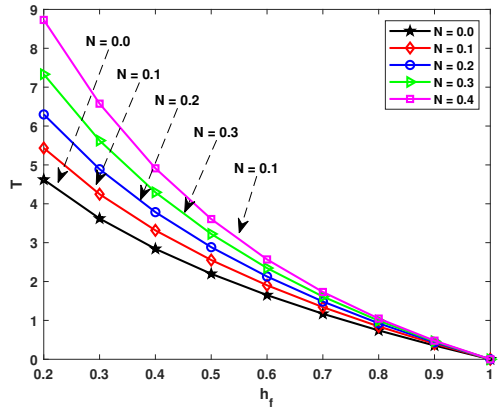

Fig. 15. Plot of dimensionless time T versus h_f for different values of N

TABLE II
COMPARISON BETWEEN POROUS AND NON POROUS CASES ON LOAD SUSTAINING CAPACITY FOR VARIOUS VALUES OF M AND N

	$\overline{h_1}$	1.2	1.4	1.6	1.8	2
ψ=0.01	N = 0.0	8.3429	8.3194	8.3007	8.2853	8.2722
	N = 0.2	10.1111	10.0759	10.0503	10.0312	10.0166
	N = 0.4	10.8439	10.8004	10.7735	10.7570	10.7473
ψ=0.0	N = 0.1	10.3681	10.3335	10.3075	10.2872	10.2709
	N = 0.2	11.1986	11.1577	11.1287	11.1075	11.0915
	N = 0.4	11.8095	11.7608	11.7314	11.7136	11.7032
ψ=0.01	M = 0	0.6993	0.6917	0.6862	0.6820	0.6788
	M= 3	3.8037	3.7740	3.7512	3.7331	3.7184
	M= 5	8.5123	8.4449	8.3889	8.3411	8.2997
ψ=0.0	M = 0	2.0694	2.0520	2.0391	2.0291	2.0212
	M= 3	4.2035	4.1689	4.1429	4.1227	4.1064
	M= 5	10.8142	10.7168	10.6406	10.5786	10.5270

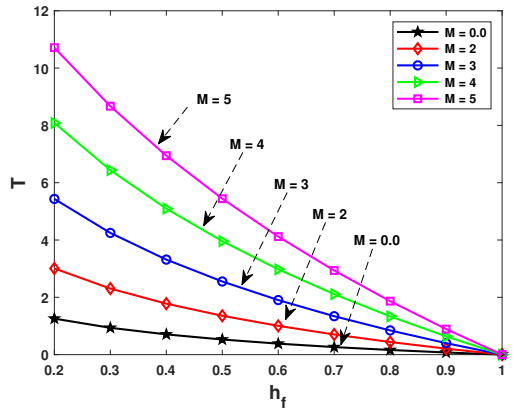

Fig. 16. Plot of dimensionless time T versus h_f for different values of M

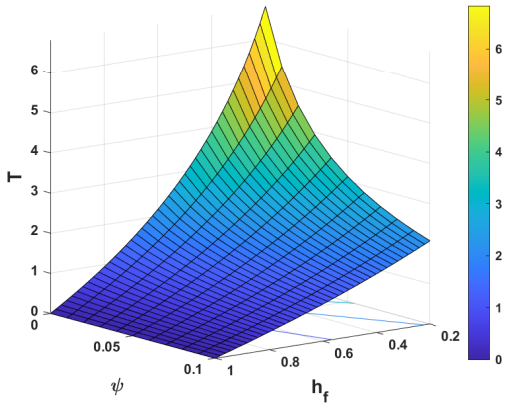

Fig. 17. Surface plot of dimensionless time T by varying h_f and ψ

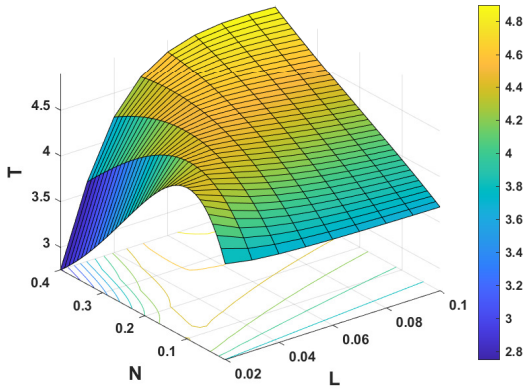

Fig. 18. Surface plot of dimensionless time T by varying L and M

sustaining capacity decreases with an increase in the value of K. Fig 7 depicts that the increase in value of L increases the load sustaining capacity. Fig 8 shows the variation of non-dimensional workload with $\overline{h_1}$ for various coupling number N values. As the coupling number increases, so does the workload. Fig 9 depicts the graph of non-dimensional load W versus $\overline{h_1}$ for different values of Hartman number. The load increases as the Hartman number value M rises. Fig 10 depicts the variation between the load sustaining capacity W and the permeability ψ for different values of film thickness $\overline{h_1}$. It is noted that when increasing the parameters $\overline{h_1}$ and

TABLE III
COMPARISON BETWEEN POROUS AND NON POROUS CASES ON SQUEEZING TIME FOR VARIOUS VALUES OF k AND L

h_f		0.2	0.4	0.6	0.8
ψ= 0.01	L = 0.04	1.6906	1.3143	0.9027	0.4617
	L = 0.06	2.1885	1.7358	1.2008	0.6164
	L = 0.08	2.5089	1.9920	1.3762	0.7054
ψ= 0.0	L = 0.04	1.7596	1.3698	0.9419	0.4822
	L = 0.06	2.3066	1.8340	1.2712	0.6535
	L = 0.08	2.6654	2.1224	1.4695	0.7544
ψ= 0.01	K = 0.6	8.2966	4.7134	2.4894	1.0254
	K = 0.7	7.5840	4.3849	2.3594	0.9903
	K = 0.8	6.4909	3.8810	2.1599	0.9366
ψ= 0.0	K = 0.6	11.5103	5.7185	2.8434	1.1351
	K = 0.7	10.4125	5.2813	2.6819	1.0932
	K = 0.8	8.7286	4.6107	2.4342	1.0290

TABLE IV
COMPARISON BETWEEN POROUS AND NON POROUS CASES ON SQUEEZING TIME FOR VARIOUS VALUES OF M AND N

h_f		0.2	0.4	0.6	0.8
ψ= 0.01	N = 0.0	4.6222	2.8407	1.6505	0.7422
	N = 0.2	6.2988	3.7851	2.1297	0.9267
	N = 0.4	8.7293	4.9129	2.5683	1.0466
ψ= 0.0	N = 0.0	5.6091	3.2592	1.8490	0.8201
	N = 0.2	8.2049	4.5225	2.4471	1.0411
	N = 0.4	12.1769	5.9839	2.9415	1.1606
ψ= 0.01	M = 0	1.2563	0.7061	0.3835	0.1624
	M = 3	5.4339	3.3168	1.9039	0.8449
	M = 5	10.7125	6.9415	4.1194	1.8662
ψ= 0.0	M = 0	1.3248	0.7301	0.3933	0.1658
	M = 3	6.8472	3.8965	2.1686	0.9452
	M = 5	17.5085	10.0143	5.5892	2.4372

ψ, the load decreases. The load carrying capacity is analysed by varying the parameters ψ and M, which is shown as the surf plot in Fig.11. It is observed from that the plates load carrying is become very high, when the absences of porosity and the presences of highly influenced MHD. If both permeability and Hartman number increases then the load carrying capacity of the plate is also increase. The load carrying capacity is analysed by varying the parameters L and N, which is shown as the surf plot in Fig.12. It is observed from that, If both characteristic material length and coupling number increases then the load carrying capacity of the plate is also increase. If both characteristic material length and coupling number decreases then the load carrying capacity of the plate is also decrease.

The comparison between the presence of porosity ($\psi = 0.01$) and absence of porosity ($\psi = 0$) for the load-sustaining capacity of the bearing is shown in Tables I and II for different values of step height K, characteristic length L, and coupling number N, Hartman number M respectively. It is found in both Tables I and II that the load sustaining capacity is more efficient in the case $\psi = 0$ than $\psi = 0.01$.

C. Dimensionless Squeeze-film time

The squeezing time varies with the significant film thickness to h_f. Fig 15 depicts the variation of dimensionless squeeze film time T with final film thickness h_f for various values of coupling number N. Fig 15 shows that as the value of N increases, squeeze time also increases. Fig 13 shows the graph of dimensionless squeeze film time T versus h_f for various step height K values. In that case, the squeeze film time decreases as the value of K increases. Fig 14 shows the variation of dimensionless squeeze film time T with h_f for various L values. It is noticed that with an increase in the value of L, the squeezing time T increases. Fig 16 shows the variation of dimensionless squeeze film time T with h_f for various M values. It is noticed that an increase in the value of Hartman number M increases the squeezing time. Fig 17 depicts the variation between the squeezing time T and the film thickness $\overline{h_1}$ for different values of permeability ψ It is noted that the squeezing time decreases when increasing the parameters $\overline{h_1}$ and ψ. The squeezing time is analysed by varying the parameters L and N, which is shown as the surf plot in Fig.18. It is observed from that, If both characteristic material length and coupling number increases then the squeezing time of the plate is also increase. The squeezing time is decreases highly, when the coupling number gets higher value and characteristic material length gets lower value.

The comparison between the presence of porosity ($\psi = 0.01$) and absence of porosity ($\psi = 0$) for the squeeze film time of the bearing is shown in Tables III and IV for different values of step height K, characteristic length L, and coupling number N, Hartman number M respectively. It is found from both Tables III and IV that the squeezing time is less in the case $\psi = 0$ than $\psi = 0.01$, the reason being requirement of more time to squeeze out the lubricant that as filled the pores when compared to solid geometry (non-porous case).

D. Estimation of relative percentage of load sustaining capacity R_W and R_T squeeze film time

The relative percentage is defined as

$$R_W = \left\{ \left(\frac{W_{\psi=0.01} - W_{\psi=0.0}}{W_{\psi=0.0}} \right) \times 100 \right\}$$

and

$$R_T = \left\{ \left(\frac{T_{\psi=0.01} - T_{\psi=0.0}}{T_{\psi=0.0}} \right) \times 100 \right\}$$

The relative percentage of load-sustaining capacity and squeeze film time are analyzed based on the presence of porosity ($\psi = 0.01$) and absence of porosity ($\psi = 0.0$). It is analyzed for the different values of film thickness $\overline{h_1}$, bearing step height K, and Hartman number M. From Table V, it is noted that the relative percentage of load sustaining capacity R_W decreases while increasing bearing step height K. However, as the Hartman number M increases, R_W increases. From Table VI it is noted that the relative percentage of squeezing time R_T decreases while increasing bearing step height K. However, as the Hartman number M increases, R_T increases.

IV. Conclusion

This study looks into how micropolar fluids and magnetic fields affect the squeeze film lubrication of porous circular stepped plates. The effect of the pressure P, load sustaining capacity W, and squeezing time T of the bearing is analyzed by varying the highly influenced parameters like $k, N, L, M, \psi, \overline{h_1}$ and h_f. The impact of porosity is observed in both scenarios of the presence ($\psi = 0.01$) and absence ($\psi = 0$) of porous materials, and the following conclusions can be drawn from the results.:

TABLE V
CHANGE IN R_W FOR DIFFERENT VALUES OF $K = 0.5, 0.7, 0.9$ AND $M = 0, 2, 3$

$\overline{h_1}$	K	R_W	M	R_W
1.2	0.6	-8.0102	0	-1.7515
	0.7	-7.8223	2	-4.9211
	0.8	-7.5094	3	-9.5116
1.4	0.6	-7.9523	0	-1.7445
	0.7	-7.7013	2	-4.9003
	0.8	-7.2595	3	-9.4723
1.6	0.6	-7.9427	0	-1.7435
	0.7	-7.6757	2	-4.8915
	0.8	-7.1883	3	-9.4546

TABLE VI
CHANGE IN R_T FOR DIFFERENT VALUES OF $K = 0.5, 0.7, 0.9$ AND $M = 0, 2, 3$

h_f	K	R_T	M	R_T
0.2	0.6	-27.920	0	-5.175
	0.7	-27.165	2	-11.707
	0.8	-25.636	3	-20.641
0.4	0.6	-17.576	0	-3.292
	0.7	-16.973	2	-8.040
	0.8	-15.827	3	-14.877
0.6	0.6	-12.451	0	-2.501
	0.7	-12.027	2	-6.455
	0.8	-11.269	3	-12.204

- The dimensionless pressure increases by increasing the value of the Hartman number M.
- The dimensionless pressure is directly proportional to the value of Hartman number M, characteristic length L, and coupling number N but it is inversely proportional to the value of step size ψ.
- In the presence of porous facing on the bearing surface, the load-sustaining capacity W and squeeze film time T both lose more efficiency than in the absence of porous.
- The load carrying capacity is directly proportional to the value of Hartman number M, characteristic length L, and coupling number N but it is inversely proportional to the value of step size K.
- The squeezing time is directly proportional to the value of Hartman number M, Coupling number N and characteristic length L, but it is inversely proportional to the value of step size K.
- Increasing the bearing film thickness height $\overline{h_1}$, the load sustaining capacity W decreases.
- Increasing the bearing final film height h_f, the squeezing film time T decreases.
- The relative percentage of squeezing time R_T directly proportional to the bearing step height K and indirectly proportional to Hartman number M.
- The relative percentage of load carrying capacity R_W directly proportional to the bearing step height K and indirectly proportional to Hartman number M.

REFERENCES

[1] Jaesung Jang and Seung S Lee, "Theoretical and experimental study of MHD (magnetohydrodynamic) micropump," Sensors and Actuators, vol. 80, pp 84–89, 2000.

[2] Bujurke N M and Kudenatti R B, "MHD lubrication flow between rough rectangular plates," Fluid Dynamics Research, vol. 39, pp 334–345, 2007.

[3] Jaw Ren Lin, "Magneto-hydrodynamic squeeze film characteristics between annular disks," Industrial Lubrication and Tribology, vol. 53, no. 2, pp 66-71, 2001.

[4] Hayat T, Nawaz M, Awatif A Hendi and Asghar S, "MHD Squeezing Flow of a Micropolar Fluid Between Parallel Disks," Journal of Fluids Engineering, vol. 133, pp 111206-1, 2011.

[5] Cemal Eringen A, "Theory of Micropolar Fluids," Journal of Mathematics and Mechanics, vol. 16, no. 1, 1966.

[6] Ian Papautsky, John Brazzle, Timothy Ameel, Bruno Frazier A, "Laminar fluid behavior in microchannels using micropolar fluid theory," Sensors and Actuators, vol. 73, pp 101–108, 1999.

[7] Pankaj Khatak and Garg HC, "Influence of micropolar lubricant on bearings performance," Proc IMechE Part J: J Engineering Tribology, vol. 226, no. 9, 2014.

[8] Johny Anthony, Sujatha Elamparithi, "Effect of MHD and surface roughness on porous step-slider bearing lubricated with couple-stress fluid," International Journal of Heat and Technology, Vol. 41, no. 1, pp 135-142, 2023.

[9] Biplab Bhattacharjee, Prasun Chakraborti, Kishan Choudhuri, "Theoretical analysis of single-layered porous short journal bearing under the lubrication of micropolar fuid," Journal of the Brazilian Society of Mechanical Sciences and Engineering, vol. 41, no. 365, pp 1-9, 2019.

[10] Naduvinamani N B and Santosh S, "Micropolar fluid squeeze film lubrication of finite porous journal bearing," Tribology International, vol. 44, pp 409-416, 2011.

[11] Naduvinamani N B, Siddangouda A, "Squeeze film lubrication between circular stepped plates of couple stress fluids," Journal of the Brazilian Society of Mechanical Sciences and Engineering, vol. 31, pp 21-26, 2009.

[12] Rajesh C Shah, "Ferrofluid lubrication of porous-rough circular squeeze film bearings," European Physical Journal Plus, vol. 137, no. 2, pp 1-16, 2022.

[13] Naduvinamani N B and Shridevi S,"Squeeze film lubrication between porous parallel plates with Magneto-Hydrodynamic Micropolar fluid," Journal of Nanofluid, vol. 7, no. 6, pp 1233–1239, 2018.

[14] Birendra Murmu and Pentyala Srinivasa Rao, "Influence of surface roughness and pressure-dependent viscosity on load carrying mechanism in micropolar fluid squeeze film lubrication between circular stepped plates," Jurnal Tribologi, vol. 25, pp 146-166, 2020.

[15] Hanumagowda B N, Shivakumar H M, Raju B T and Santhosh Kumar J, "Combined effect of Pressure-dependent viscosity and micropolar fluids on squeeze film circular stepped plates," International Journal of Mathematics Trends and Technology, vol. 37, no. 3, pp 175-183, 2016.

[16] Naduvinamani N B, Hanumagowda B N, Syeda Tasneem Fathima "Combined effects of MHD and surface roughness on couple-stress squeeze film lubrication between porous circular stepped plates," Tribology International, vol. 56, pp 19-29, 2012.

[17] Faisal Salah, and Mubarak H. Elhafian, "Numerical Solution for Heat Transfer of Non - Newtonian Second - Grade Fluid Flow over Stretching Sheet via Successive Linearization Method," IAENG International Journal of Applied Mathematics, vol. 49, no.4, pp 505-512, 2019

[18] Brinda Halambi and Hanumagowda B N, "Micropolar squeeze film lubrication analysis between Rough porous elliptical plates and surface roughness effects under the MHD," Ilkogretim Online Elementary Education Online, vol. 20, no. 4, pp 307-319, 2021.

[19] Itishree Nayak,"Numerical Study of MHD Flow and Heat Transfer of an Unsteady Third Grade Fluid with Viscous Dissipation," IAENG International Journal of Applied Mathematics, vol. 49, no.2, pp 245-252, 2019

[20] Johny A and Sujatha E, "Effect Of Magneto Hydrodynamic Using Micro-Polar Fluid Between Circular Stepped Plate," ARPN Journal of Engineering and Applied Sciences, vol. 18, no. 5, pp 543-548, 2023.

[21] Sangeetha Sekar, Sujatha Elamparithi, Sivakami Lakshmi Nathan and Lakshmi Priya Saravanathan, "Effect of MHD with micropolar fluid between conical rough bearings," International Journal of Heat and Technology, vol. 40, no. 5, pp 1210-1216, 2022.

[22] Naduvinamani N B and Ashwini Angadi, "Magnetohydrodynamic Micropolar fluid squeeze film lubrication between stepped porous parallel plates," Indian Journal of Science and Technology, vol. 15, no. 40, pp 2066-2076, 2022.

[23] Johny A and Sujatha E, "Effect of Double Porous Layer on Rough Step Slider Bearing Lubricated with Couple Stress Fluid," Mathematical Modelling of Engineering Problems, vol. 10, no. 6, pp 2185-2192, 2023.

[24] M. Faizan Ahmed, and E. Sujatha, "Combined Effect of Surface Roughness and Magnetohydrodynamic with Micropolar Fluid between Porous Triangular Plates," IAENG International Journal of Applied Mathematics, vol. 53, no.4, pp 1266-1273, 2023